Available online at www.sciencedirect.com

ScienceDirect

Procedia CIRP 79 (2019) 21–26

www.elsevier.com/locate/procedia

12th CIRP Conference on Intelligent Computation in Manufacturing Engineering, 18-20 July 2018, Gulf of Naples, Italy

Advanced process design for re-contouring using a time-domain dynamic material removal simulation

B. Denkena[a], O. Pape[a], T. Grove[a], A. Mücke[a,*]

[a]*Institute of Production Engineering and Machine Tools (IFW), Leibniz Universität Hannover, An der Universität 2, 30823 Garbsen, Germany*

* Corresponding author. Tel.: +49-511-762-18270; fax: +49-511-762-5115. *E-mail address:* muecke@ifw.uni-hannover.de

Abstract

The repair of components often requires the removal of excess weld material. This removal is considered as re-contouring. Re-contouring processes have to be designed individually for each case of damage to fulfil the high quality requirements. Therefore, a prognosis of the machined surface topography is crucial. The material removal simulation introduced in this paper allows the prediction of process stability and surface topography for 5-axis ball end milling including dynamic effects. Different process strategies for re-contouring of Ti-6Al-4V welds are examined. It is shown, that selecting suitable process parameters can lead to high surface quality while maintaining productivity.

Peer-review under responsibility of the scientific committee of the 12th CIRP Conference on Intelligent Computation in Manufacturing Engineering.

Keywords: Titanium; Milling; Simulation

1. Introduction

High value products such as jet engines require effective maintenance, repair and overhaul services to increase economic efficiency and sustainability [1]. In the case of jet engines, components like blades, vanes or combustion chambers need specialized repair technologies to maintain or even improve their functional properties throughout the life cycle [2]. Designing these repair processes is a challenging task and differs from new part production [3]. Typically, a material deposit is needed to attach repair patches or fill cracks. Afterwards, the excess material has to be removed to restore the desired geometry. This removal is considered as re-contouring, wherefore milling processes are commonly used. The uniqueness of repair cases, different materials (e.g. base and weld material) and parts prone to vibration complicate the repair. Additionally, 5-axis machining processes are required to restore the complex part geometries and to overcome the limited accessibility e.g. while regenerating blade integrated disks (Blisks). Compared to new part production, it is hardly possible to test the process with a spare part beforehand. This leads to the necessity of a tailored and precise process planning procedure to ensure high geometric accuracy and surface quality for minimizing scrap and flow loss [4]. Due to the components' complex shapes, ball end milling is often applied. For ball end milling, there are numerous studies dealing with process design for new part production. Methods exist to predict process stability, surface topography and productivity [5]. They can be categorized into empirical, analytical and numerical methods. Usually, the approaches for predicting process stability are analytical and limited to the recommendation of stable process parameters calculating the stability lobes. The examination of the generated surface topography is not possible. Therefore, numerical simulations in time-domain are required. They are called material removal simulations (MRS) and use e.g. voxel, dexel or constructive solid geometry (CSG) to discretize the workpiece. In contrast to common analytical approaches, the numerical simulation offers advantages regarding flexibility. True milling kinematics and workpiece geometries can be used. Thus, it is possible to calculate engagement parameters even for complex geometries and tools. However, MRS are less efficient compared to analytical models [5]. Moreover, most of the numerical approaches do not consider dynamics and are restricted to the

2212-8271
Peer-review under responsibility of the scientific committee of the 12th CIRP Conference on Intelligent Computation in Manufacturing Engineering.
10.1016/j.procir.2019.02.005

calculation of static deflection. For example, Böß et al. presented a dexel based MRS, which is able to consider different material properties [6]. Nespor et al. extended this model by the consideration of tool run-out, cutting edge chipping and static tool deflection. The workpiece was considered stiff and dynamic effects were neglected [7]. One of the rare examples for a numerical time-domain simulation including tool dynamics for general milling is the approach of Surmann et al. [8]. It is based on CSG. The uncut chip thickness is obtained from the machined chip shape, which is derived from the intersection of the tool envelope and workpiece using Boolean operations. The process forces are calculated based on the Kienzle equation and applied to a system of oscillators describing the dynamic behavior of the tool [8]. Kersting et al. extended the model by considering workpiece vibrations [9]. In contrast to the previous mentioned works, the approach presented in this paper is dexel-based. Real process kinematics and tool and workpiece geometries can be used as well as different material properties. This allows the systematic design and optimization of general milling and re-contouring processes in order to minimize shape deviations and increase productivity. The tool geometry consists of a rake face geometry and flank face geometry. Consequently, they can be modeled and examined independently. Therefore, the rake- and flank face geometries are discretized by quadrilateral elements. The sweep volume of the rake face is subtracted from the workpiece to calculate the undeformed chip dimensions. Thus, process forces can be obtained using the implemented force model by Altintas [10]. Obviously, the flank face is not considered for the calculation of undeformed chip dimensions. It can be used to determine the contact conditions of the flank face with the workpiece (e.g. contact length). This can be beneficial for further modeling of process damping. Generally, process dynamics are implemented by sets of harmonic oscillators according to [9]. In this paper, the simulation has been applied to 5-axis ball end milling in order to virtually develop re-contouring strategies considering dynamic effects. The corresponding workflow and experimental setup will be described in the next chapter.

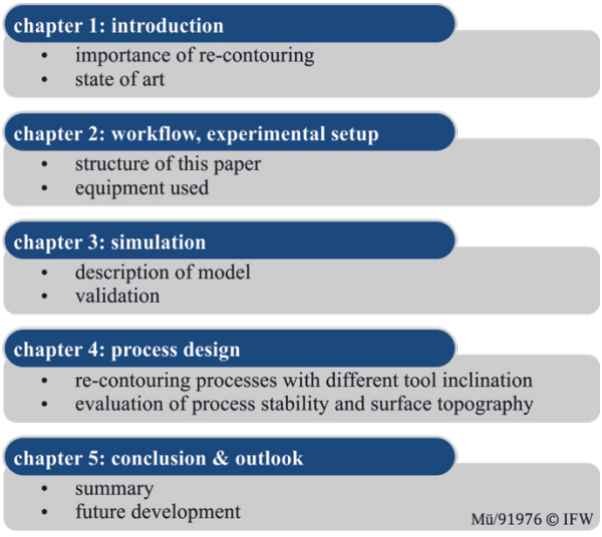

Fig. 1. Workflow of this paper

2. Workflow and experimental setup

This paper consists of five different chapters. The corresponding structure is depicted in Fig. 1. First, the introduction has been given to demonstrate the importance of re-contouring. Additionally, the current state of art regarding process simulation and design of re-contouring has been pointed out. Second, this chapter describes the structure of this paper as well as the experimental equipment used. The simulation environment with its different components is described in chapter three. An experimental validation confirms the suitability of this approach. In the fourth chapter, the simulation is used to develop different re-contouring strategies. Especially the tool inclination angles are varied to enhance the geometric accuracy. At last, a summary of this paper as well as the focus of further research is given.

To validate the developed simulation, ball end milling experiments were carried out on a Deckel Maho DMU 125P duoBlock 5-axis machine tool. Therefore, specimen made of AMS 4911 Ti-6Al-4V (90x90x10 mm³) were machined using a 10 mm Seco JH970100 ball end mill. The tool shank of the two-fluted solid carbide ball end mill was inserted into a shrink fit tool holder type Garant 30823510. The occurring process forces have been measured with a Kistler 9257B dynamometer. To obtain the modal parameters of the tool, an experimental modal analysis has been conducted. Therefore, an impact hammer type PCB Piezotronic 086C03 has been used to supply energy to the system. The vibrations were measured by a laser vibrometer system type Polytec OFV-3001 + OFV-303. The modal parameters from the frequency-response functions were determined using a genetic algorithm. To measure the surface topography, an Alicona InfiniteFocus G5 measurement system has been used. The system is based on the measurement principle of focus-variation, which is non-contact, optical and three-dimensional.

3. Material removal simulation

The material removal simulation allows the prediction of surface topography and process stability in time-domain. The consideration of tool- and workpiece dynamics allows for not only the investigation of process stability, but also for the analysis of geometrical errors and surface quality due to

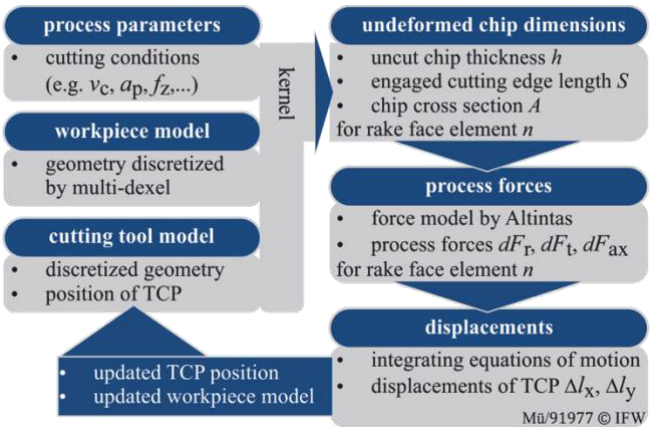

Fig. 2. Simulation structure

vibrations. The simulation structure is depicted in Fig. 2 and will be described in the next section.

3.1. Simulation setup

The simulation consists of different modules. Workpiece, cutting tool model and the process parameters have to be defined first. The workpiece geometry is discretized using a multi-dexel grid. The rake and flank face geometry, e.g. scan of actual tool geometry or CAD model (without imperfections like chipping), is segmented into elements of four nodes each. The cutting process is split into time steps i and a step size of

$$\Delta t = \frac{t_{tot}}{N} = \frac{L \cdot 60}{v_f \cdot N}, \tag{1}$$

where t_{tot} is the total time of the cutting process, N the number of time steps, L the length of the tool path and v_f the feed velocity. For each time step i, the tool rotates about the angular step $d\phi$ and the undeformed chip dimensions are calculated for each tooth and the corresponding rake face elements. This is done by subtracting the sweep volume of the tool from the workpiece using Boolean operation.

Specifically, the uncut chip thickness h, the engaged cutting edge length S and the chip cross section A are calculated. They are incorporated into the force model presented in [10], eq. 2.

$$\begin{bmatrix} dF_t \\ dF_r \\ dF_a \end{bmatrix} = \begin{bmatrix} K_{tc} \cdot dA + K_{te} \cdot dS \\ K_{rc} \cdot dA + K_{re} \cdot dS \\ K_{ac} \cdot dA + K_{ae} \cdot dS \end{bmatrix} \tag{2}$$

The differential cutting forces in tangential (dF_t), radial (dF_r) and axial (dF_a) direction are calculated for each rake face element and time step i. They are integrated over all elements to the resultant forces F_t, F_r, F_a. The material-, tool- and process- dependent force coefficients are identified mechanistically from milling tests at different feed rates according to [11]. The process forces can be transformed to the local workpiece coordinate system using a transformation matrix, c.f. [5].

Two driven damped oscillators represent the dynamic behavior of the tool with one vibration mode in x- and y-direction, eq. 3.

$$\begin{aligned} m_x \cdot \ddot{x}(t) + d_x \cdot \dot{x}(t) + c_x \cdot x(t) &= F_x(t) \\ m_y \cdot \ddot{y}(t) + d_y \cdot \dot{y}(t) + c_y \cdot y(t) &= F_y(t) \end{aligned} \tag{3}$$

The tool axis (z) is considered stiff. Although, it is possible to use an arbitrary number of oscillators for every direction. The corresponding equations of motion have the initial condition $x = \dot{x} = \ddot{x} = 0$. Then, the dynamic tool displacement at time step i+1 can be derived by numerical integration. For enhanced numerical stability, because of better energy conservation when compared to classical Euler integration, the semi-implicit Euler method is used. This leads to bigger time step sizes Δt and thus faster computation. The dynamic tool displacement at i+1 can be calculated as following:

$$\begin{bmatrix} \ddot{x}^i \\ \ddot{y}^i \end{bmatrix} = \begin{bmatrix} (F_x^i - d_x \cdot \dot{x}^i - c_x \cdot x^i) \cdot \frac{1}{m_x} \\ (F_y^i - d_y \cdot \dot{y}^i - c_y \cdot y^i) \cdot \frac{1}{m_y} \end{bmatrix} \tag{4}$$

$$\begin{bmatrix} \dot{x}^{i+1} \\ \dot{y}^{i+1} \end{bmatrix} = \begin{bmatrix} \dot{x}^i + \ddot{x}^i \cdot \Delta t \\ \dot{y}^i + \ddot{y}^i \cdot \Delta t \end{bmatrix} \tag{5}$$

$$\begin{bmatrix} x^{i+1} \\ y^{i+1} \end{bmatrix} = \begin{bmatrix} x^i + \dot{x}^{i+1} \cdot \Delta t \\ y^i + \dot{y}^{i+1} \cdot \Delta t \end{bmatrix} \tag{6}$$

Then, the dynamic displacement is added to the nominal tool center point (TCP) coordinates. The nominal tool path refers to the cutter location, e.g. given by a cutter location source file (CLSF). In this paper, a time step size of $\Delta t \approx 5 \cdot 10^{-5}$ s was sufficient for convergence. Classical Euler required a time step size of $\Delta t \approx 1 \cdot 10^{-7}\ s$. Alternatively, Runge Kutta methods could be used as well. However, the time step size is limited by the frequency spectrum to be investigated. The parameters modal mass m, damping constant d and stiffness k have to be determined in advance from frequency-response functions (FRF). It is possible to consider workpiece dynamics with this approach using the superposition principle. Simulations using the finite element method can derive the corresponding FRFs, which are time (loss of mass) and position dependent.

3.2. Validation

To validate the proposed approach, slot milling experiments have been performed with a long and slender tool and stiff workpieces from Ti-6Al-4V. Different depth of cuts a_p were used to realize stable, semi stable and instable processes using the process parameters listed in Fig 3. The tool orientation is described by the projected angles lead angle λ and tilt angle τ [7]. An experimental modal analysis has been performed to determine the modal parameters of the tool. They are listed in table 1.

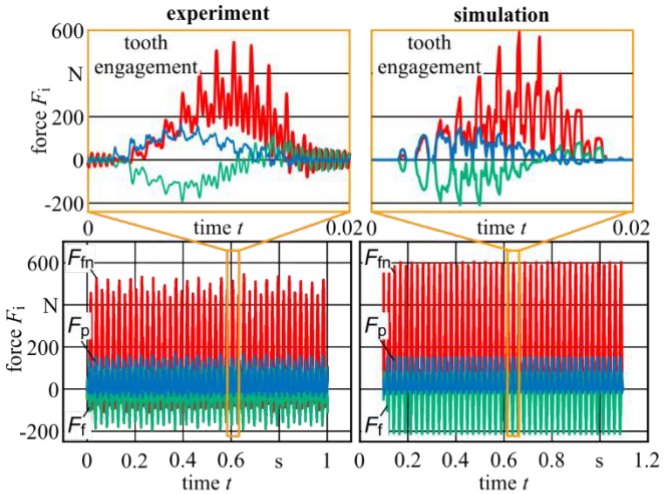

Fig. 3. Experimental (left) and simulated (right) process forces for an unstable process

Table 1. Modal parameters for the slender ball end mill.

parameter	x-direction (cross feed)	y-direction (feed)
modal mass *m*	0.2316 kg	0.2125 kg
stiffness *k*	4252868 N/m	3982039 N/m
damping constant d	28.98 Ns/m	18.79 Ns/m

The force signal has been analyzed regarding its frequency spectrum. Additionally, the surface topographies are considered. In this case, the simulation uses an ideal tool based on the real geometry, without imperfections such as cutting edge chipping. The dexel resolution was set to 1000x1000x1000 in x-, y- and z-direction to discretize the virtual workpiece, which size is 5x8x1 mm^3. Exemplarily, an instable process is shown in Fig. 3. It can be seen that the simulated process forces are in good agreement with the measured data. Differences occur regarding the maximum forces as well as the fluctuation of the signal, because the tool run-out has been neglected in the simulation. Additionally, process damping of the flank face is not modeled. The tooth engagements show comparable frequency characteristics. Similar harmonics are visible during the tooth engagement. The different decay of the experimental tooth engagement can be referred to the eigenfrequency of the dynamometer. The frequency spectrum derived by Fast Fourier Transform (FFT) is shown in Fig. 4 and proves this statement as well as the capability of the simulation. The chatter frequencies are predicted adequately. Only small differences occur. The eigenfrequency of the dynamometer can be seen at 2.2 kHz, which is in line with the eigenfrequency stated by the manufacturer.

In Fig. 5, the surface topographies are shown. Obviously, they resemble each other in appearance, because of the similar chatter frequencies. However, the chatter marks vary in depth because of the missing process damping. Further deviations occur due to the ideal tool geometry without edge chipping as well as the missing of ploughing effects. For all tested cutting parameters, the simulation and experiments were in good agreement. In the next chapter, the simulation will be used to optimize a re-contouring process of stiff workpieces by varying tool orientation and cutting speed using a long and slender tool holder.

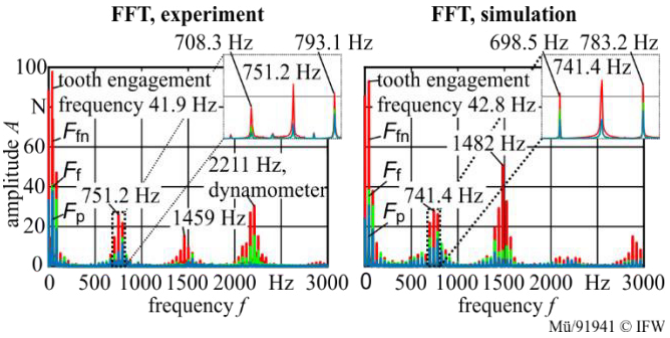

Fig. 4. Frequency spectrum of measured and simulated force signal

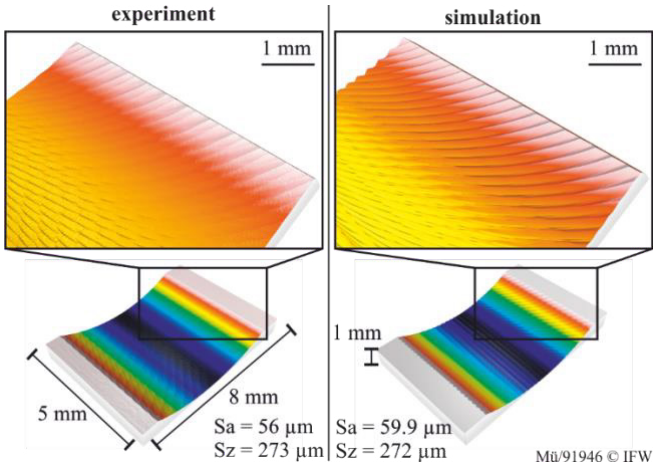

Fig. 5. Comparison of measured surface topography (left) and simulated topography (right) for an instable process

4. Process design for re-contouring

As a use case, a stiff workpiece containing a weld has been virtually re-contoured using a long and slender tool holder. Three different tool inclination angles and cutting speeds were investigated resulting in nine different factor combinations. The equipment described in chapter 2 has been used. For all inclination angles, cutting force coefficients have been mechanistically identified separately. Therefore, slot milling experiments of Ti-6Al-4V workpieces at different feed rates were performed. For the weld material, the cutting force coefficients were identical to the base material. This is suitable for conventional tungsten inert gas (TIG) welds as shown in [12]. The virtual model of the ball end mill features the same macro-geometry of the actual tool. No edge chipping has been considered, the cutting edge is sharp. The workpiece dimensions are shown in Fig. 6. The maximum height of the weld is h_s = 0.5 mm. Only one finishing operation is executed to re-contour the workpiece, thus the maximum occurring depth of cut a_p corresponds to h_s. The workpiece has been discretized by 1000x1000x1000 dexel in each direction x, y, z. The process parameters are summarized in table 2.

Table 2. Process parameters for re-contouring use case.

parameter	value
material	Ti-6Al-4V
weld size (height, width)	0.5 x 3.87 mm
feed per tooth f_z	0.12 mm
step over b_r	0.5 mm
cutting speed v_c	40, 120, 160 m/min
cutting edge radius r_β	4 µm
tool inclination lead angle λ / tilt angle τ	15, 30, 55 / 0°
depth of cut a_p	0.5 mm

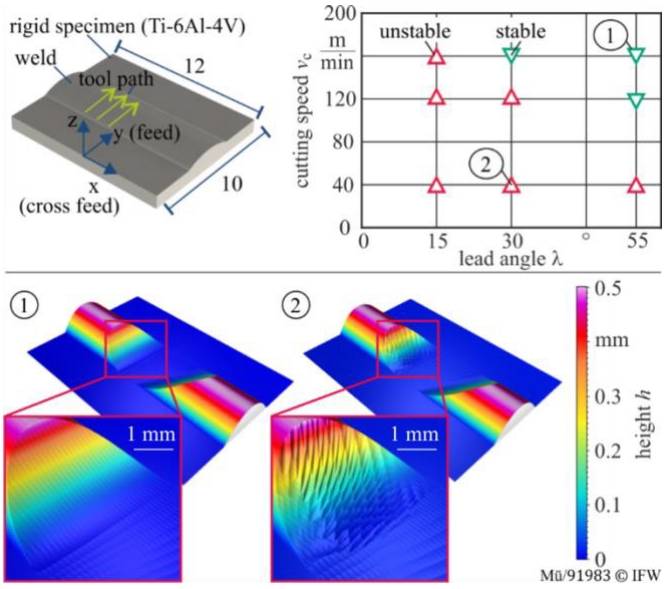

Fig. 6. Process stability for all factor combinations and surface topographies of the re-contoured workpieces.

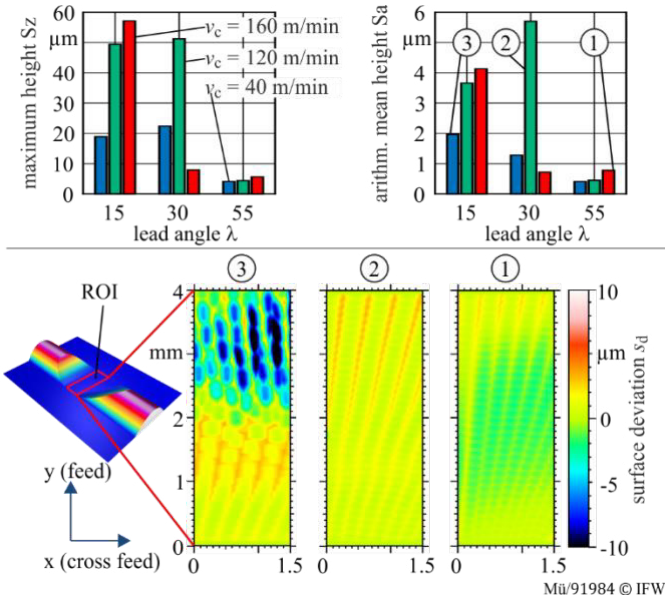

Fig. 7. Surface quality and surface deviation

In Figure 6, the process stability of the factor combinations and exemplary surface topographies are shown. For all considered parameters, stable processes are only observed for λ = 55° at v_c = 120 m/min and 160 m/min as well as λ = 30° at v_c = 160 m/min. Using a lead angle of λ = 15°, the process was unstable for all considered cutting speeds. Especially the first cut is crucial, where the tool is performing a slot milling operation when entering the weld. During this operation, the highest process forces and tool displacements occurred. Exemplarily shown for case 2 (λ = 30°, v_c = 40 m/min) in Fig. 6, chatter marks may result on the flank of the groove. The following cuts with a step over b_r = 0.5 mm (down milling) are less critical, because of the smaller cross-section of undeformed chip resulting in smaller process forces and thus in less excitation of the tool. For case 1 (λ = 55°, v_c = 160 m/min), even during slot milling the process was stable. No chatter marks could be observed on the flank of the groove as shown at the bottom left of Fig. 6. Thus, selecting appropriate lead angles λ can be beneficial to improve process stability with respect to the limited accessibility while e.g. performing a Blisk repair. For all conducted simulations, the surface roughness of the re-contoured region has been analyzed by exporting the virtually machined workpiece to the software µsoft analysis from nanofocus. Amongst others, the software allows the calculation of the height parameters Sa (arithmetical mean height of the surface) and Sz (maximum height of the surface), which were used to evaluate surface quality. They are shown in Fig. 7 for all factor combinations. The region of interest (ROI) is characterized by a red rectangle in the lower left of Fig. 7. Obviously, the stable processes show the best surface quality. Both Sz and Sa are minimal for λ = 55° at all cutting speeds and λ = 30°, v_c = 160 m/min. However, the combination λ = 55°, v_c = 40 m/min was unstable during slot milling of the weld as depicted in Fig. 6. At the bottom of Fig. 7, the surface deviation s_d is shown for case 1, 2 and 3. In this context, s_d is zero for the unmachined base material. Case 1 and case 2 show only a minimal surface deviation, whereas case 3 is undersized up to 10 µm. This can be referred to the greater amplitude of vibration of the tool normal to the surface. The trajectories of the TCP in the x-y and x-z plane of the workpiece coordinate system are shown in Fig. 8 during one following cut (down milling) along with the corresponding frequency spectrum. For case 3 shown on the left of Fig. 7, the TCP trajectories in both planes underline the instability, leading to direct surface errors as depicted in Fig. 7. Accordingly, the trajectories of the stable process (case 1) are less pronounced. In the frequency spectrum, the amplitudes of the tooth engagement frequencies (case 3: f = 42.8 Hz, case 1: f = 165.1 Hz) are visible besides

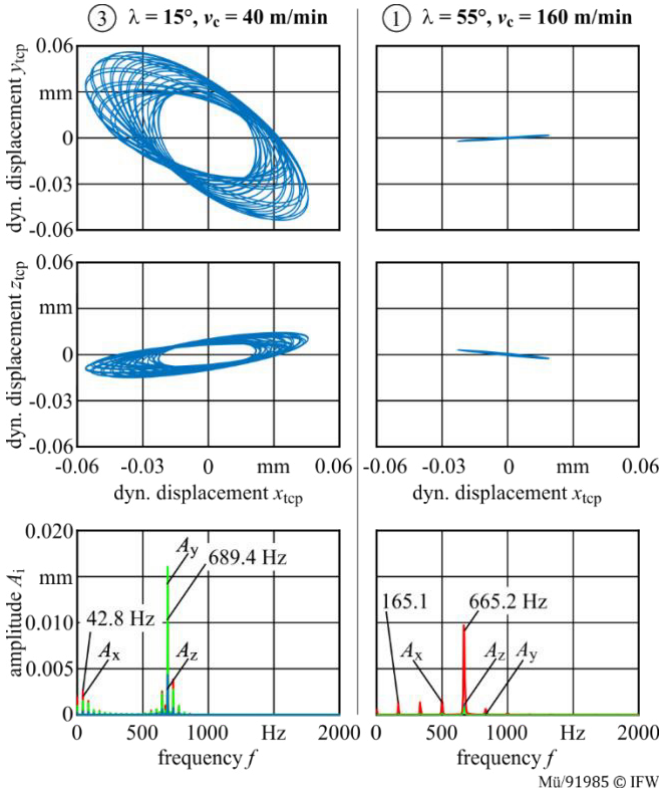

Fig. 8. Displacement of TCP in x-y and x-z plane during one following cut and frequency spectrum for case 1 and 3 in workpiece coordinate system.

the amplitudes of chatter frequencies near the eigenfrequencies of the tool. Because of the stiff considered tool axis, the amplitude in y-direction (feed) is comparably small for case 1. In this case, the tool is more inclined towards feed direction leading to vibrations in the x-z plane of the workpiece coordinate system mainly.

5. Conclusion and outlook

In this paper, a time-domain dynamic material removal simulation has been developed and experimentally validated. A use case demonstrated the ability of the simulation to design and optimize re-contouring processes. Thus, shape deviations can be reduced and productivity increased by virtually investigating the effects of process parameters on the process forces and machined surface topography.

Using harmonic oscillators derived from frequency response functions, the simulation allows considering dynamic effects for arbitrary tool- and workpiece geometries. Additionally, true kinematics are used. In future work, further relevant factors influencing the surface topography will be considered such as run-out and edge chipping. This can be done by importing real measured tool geometry into the simulation. Additionally, the implementation of process damping is important for an advanced prognosis. Therefore, the simulation offers the opportunity to determine contact conditions of the flank face with the workpiece. Especially for re-contouring processes featuring low cutting speeds, e.g. the machining of hard-to-cut materials such as superalloys (e.g. Inconel) or titanium alloys, the effect of process damping on process stability increases as known from literature [13]. Then, the decreased amplitudes will also influence e.g. the depth of chatter marks on the surface. Thus, modeling the process damping of the flank face will lead to an enhanced prediction of surface topography.

Acknowledgements

The authors kindly thank the German Research Foundation (DFG) for the financial support of the Collaborative Research Center (SFB) 871 “Regeneration of Complex Capital Goods” which provides the opportunity of their collaboration in the research projects B2 “Dexterous Regeneration Cell” and C1 “Simulation Based Planning of Re-contouring Metal Cutting Processes”.

References

[1] Uhlmann E, Bilz M, Baumgarten J. MRO – Challenge and Chance for Sustainable Enterprises. Procedia CIRP 11 2013;239:344.
[2] Eberlein A. Phases of high-tech repair implementation. 18th International Symposium on Airbreathing Engines (ISABE) 2007.
[3] Denkena B, Boess V, Nespor D, Floeter F, Rust F. Engine blade regeneration: a literature review on common technologies in terms of machining. The International Journal of Advanced Manufacturing Technology 2015;81:917.
[4] Bons JP. A review of surface roughness effects in gas turbines. Journal of Turbomachinery 2010;132(2):021004-16.
[5] Altintas Y, Kersting P, Biermann D, Budak E, Denkena B, Lazoglu I. Virtual process systems for part machining operations. CIRP Annals – Manufacturing Technology 2014;63:585-605.
[6] Böß V, Nespor D, Samp A, Denkena B. Numerical simulation of process forces during re-contouring of welded parts considering different material properties. CIRP Journal of Manufacturing Science and Technology 2013;6(3):167-174.
[7] Nespor D, Denkena B, Grove T, Pape O. Surface topography after re-contouring of welded Ti-6Al-4V parts by means of 5-axis ball nose end milling. The International Journal of Advanced Manufacturing Technology 2016;85:1585.
[8] Surmann T, Biermann D. The effect of tool vibrations on the flank surface created by peripheral milling. CIRP Annals 2008;57(1):375-378.
[9] Wiederkehr P, Biermann D. Modeling workpiece dynamics using sets of decoupled oscillator models. Machining Science and Technology 2012:16(4):564-579.
[10] Engin S, Altintas Y. Mechanics and dynamics of general milling cutters. International Journal of Machine Tools and Manufacture 2011;41:2195.
[11] Gradisek J, Kalveram M, Weinert K. Mechanistic identification of specific force coefficients for a general end mill. International Journal of Machine Tools and Manufacture 2004;44:401-414.
[12] Denkena B, Mücke A, Schumacher T, Langen D, Grove T, Bergmann B, Hassel T. Ball end milling of titanium TIG weld material and the effect of SiC addition – process forces and shape deviations. 6th International Conference on Through-life Engineering Services 2017, Procedia Manufacturing 2018;19:74-81.
[13] Budak E, Tunc LT. Identification and modeling of process damping in turning and milling using a new approach. CIRP Annals 2010;59:403-408.